



## Pressure-induced quantum phase transition in $\text{Fe}_{1-x}\text{Co}_x\text{Si}$ ( $x = 0.1, 0.2$ )

M. K. Forthaus,<sup>1</sup> G. R. Hearne,<sup>2</sup> N. Manyala,<sup>3</sup> O. Heyer,<sup>1</sup> R. A. Brand,<sup>4</sup> D. I. Khomskii,<sup>1</sup> T. Lorenz,<sup>1</sup> and M. M. Abd-Elmeguid<sup>1</sup>

<sup>1</sup>*II. Physikalisches Institut, Universität zu Köln, Zùlpicher Str. 77, D-50937 Köln, Germany*

<sup>2</sup>*Department of Physics, University of Johannesburg, P.O. Box 524, Auckland Park, Johannesburg, RSA*

<sup>3</sup>*Department of Physics, Institute of Applied Materials, University of Pretoria, Pretoria, RSA*

<sup>4</sup>*Karlsruher Institut für Technologie (KIT), Institut für Nanotechnologie (INT), Hermann-von-Helmholtz-Platz 1, D-76344 Eggenstein-Leopoldshafen, Germany*

(Received 21 June 2010; revised manuscript received 7 December 2010; published 2 February 2011)

We have investigated the effect of pressure on electrical transport and magnetic properties of ferromagnetic  $\text{Fe}_{1-x}\text{Co}_x\text{Si}$  alloys for  $x = 0.1$  ( $T_C \sim 11$  K) and  $x = 0.2$  ( $T_C \sim 32$  K) using electrical resistivity measurements up to about 30 GPa. We have also studied the magnetic properties of these samples ( $x = 0.1$  and  $x = 0.2$ ) and a sample with  $x = 0.3$  ( $T_C \sim 43$  K) at ambient pressure using  $^{57}\text{Fe}$  Mössbauer-effect (ME) spectroscopy. The ME results indicate that the effective magnetic hyperfine field  $B_{\text{eff}}$  at the  $^{57}\text{Fe}$  nucleus exhibits the same concentration dependence as the macroscopic magnetic moment and confirm that the onset of magnetic order is above  $x \sim 0.02$ . The analysis of the high-pressure results reveals in both samples a gradual suppression of the ferromagnetic state to a quantum phase transition (QPT) at pressures of  $p \sim 11$  GPa and  $p \sim 12$  GPa for  $x = 0.1$  and  $x = 0.2$ , respectively. High-pressure x-ray diffraction measurements on the three samples indicate very similar change of the volume of the cubic unit cell with pressure and exclude that the observed QPTs are connected with a structural phase transition. We discuss the observed instability of the ferromagnetic state with increasing Co concentration in the context of increasing local crystallographic disorder, which causes a change of the distribution of the helix wave vector as well as a modification of the ferromagnetic half-metallic state. We further show that, in the pressure-induced nonmagnetic metallic state, all samples, regardless of their different local crystallographic disorder, exhibit similar non-Fermi-liquid behavior [ $\rho(T) \propto T$ ]. Finally, we find a small but positive magnetoresistance in the high-pressure metallic state well beyond the QPT of  $\text{Fe}_{0.9}\text{Co}_{0.1}\text{Si}$ . This can be attributed to a slight field-induced modification of the spin majority and minority band which leads to a very small magnetic moment.

DOI: [10.1103/PhysRevB.83.085101](https://doi.org/10.1103/PhysRevB.83.085101)

PACS number(s): 71.30.+h, 75.30.Kz, 75.50.Bb

### I. INTRODUCTION

In recent years, the disordered  $\text{Fe}_{1-x}\text{Co}_x\text{Si}$  alloys, crystallizing in the cubic B20-type structure, have attracted significant interest due to their remarkable electronic and magnetic properties.<sup>1-10</sup> The undoped system FeSi is a paramagnetic metal at high temperatures ( $T \gtrsim 400$  K). However, its electrical resistivity increases dramatically with decreasing temperature, yielding an insulating ground state.<sup>11,12</sup> The opening of a small energy gap (around 60 meV) at low temperatures has been observed.<sup>13,14</sup> On the other hand, investigations of the magnetic properties of FeSi have revealed that the ground state is nonmagnetic: although the magnetic susceptibility above 500 K indicates a local moment behavior, no long-range magnetic order has been detected by neutron diffraction,<sup>29</sup> Si nuclear magnetic resonance, and  $^{57}\text{Fe}$  Mössbauer experiments at low temperatures.<sup>15,16</sup> Because of these findings, FeSi has been characterized as a narrow-gap semiconductor and, therefore, was considered as a candidate for a 3d-based Kondo insulator.<sup>17</sup> However, this scenario has been put into question by very recent photoemission spectroscopy measurements that suggest that FeSi is most appropriately described as an itinerant semiconductor.<sup>18-20</sup>

Most interesting is the finding that a slight substitution of Fe by Co (i.e., electron doping) induces a metal-insulator transition at about  $x \simeq 0.02$ .<sup>1</sup> Higher Co doping ( $0.05 \leq x \leq 0.7$ ) leads to the formation of an unusual ferromagnetic metallic state which exhibits a helical magnetic structure<sup>2,3</sup> similar to that reported for the isostructural compounds MnSi<sup>21,22</sup>

and FeGe.<sup>23,24</sup> According to the magnetic phase diagram of  $\text{Fe}_{1-x}\text{Co}_x\text{Si}$ ,<sup>4,5</sup> the onset of ferromagnetic order is for  $x \gtrsim 0.05$  with a maximum ordering temperature ( $T_C \sim 50$  K) for  $x = 0.4$ . Upon further increasing Co concentration, the magnetic state is suppressed, since the end member of the series (CoSi) is a diamagnetic compound. The saturation magnetization  $M$  has been shown to follow  $T_C$  in the whole concentration range. Here,  $M$  linearly increases with increasing  $x$  below  $x \simeq 0.2$  and saturates at low external magnetic fields ( $B \lesssim 0.2$  T).<sup>5</sup> This behavior suggests that the excess 3d electrons only occupy the majority spin band.<sup>5,6</sup> Moreover, a positive magnetoresistance has been reported. These observations have been attributed to the nearly-half-metallic nature of  $\text{Fe}_{1-x}\text{Co}_x\text{Si}$ , in which the electrons responsible for ferromagnetism are triggering the electrical and magnetotransport.<sup>5,6</sup>

A promising approach for a better understanding of such a strong coupling between the spin and charge degrees of freedom in this system is to investigate the effect of external pressure  $p$  on the magnetic and electrical transport properties of  $\text{Fe}_{1-x}\text{Co}_x\text{Si}$  at fixed concentrations. Indeed, recent high-pressure studies on a ferromagnetic metallic  $\text{Fe}_{0.7}\text{Co}_{0.3}\text{Si}$  sample ( $T_C \sim 43$  K) revealed a complete suppression of the ferromagnetic order and a transition to a nonmagnetic state above a critical pressure  $p_c$  of about 7 GPa<sup>5</sup> [i.e., magnetic quantum phase transition (QPT)]. Most interesting is the observation of an unusual temperature dependence of the electrical resistivity [ $\rho(T) \propto T$ ] at low temperatures from  $p_c = 7$  GPa to 10 GPa. This is entirely different from that reported for MnSi and FeGe [ $\rho(T) \propto T^{3/2}$ ] at and beyond

$p_c$ .<sup>25–28</sup> A possible origin for the linear behavior of  $\rho(T)$  in  $\text{Fe}_{0.7}\text{Co}_{0.3}\text{Si}$  has been attributed to the existence of chemical (atomic) disorder in the sample.<sup>5</sup>

In fact, recently experimental evidence for local crystallographic Co-Fe site disorder in  $\text{Fe}_{1-x}\text{Co}_x\text{Si}$  has been reported. Raman spectroscopy data shows a clear increase of the Raman line width as the Co concentration increases with a maximum at  $x = 0.5$ .<sup>9</sup> Furthermore, small-angle polarized neutron diffraction measurements reveal that the helix wave vector exhibits a distribution which increases with increasing Co concentration.<sup>10</sup> Finally, *ab initio* calculations on  $\text{Fe}_{1-x}\text{Co}_x\text{Si}$  indicate that these alloys behave as a disordered ferromagnetic half-metal and that increasing disorder with increasing Co concentration results in a gradual suppression of the half-metallic character.<sup>6</sup>

Motivated by such unusual behavior of these disordered alloys, and in particular the observed anomalous metallic nonmagnetic state under high pressure, we have investigated the effect of pressure on the electronic, magnetic, and structural properties in much less crystallographically disordered  $\text{Fe}_{0.9}\text{Co}_{0.1}\text{Si}$  ( $T_C \sim 11$  K) and  $\text{Fe}_{0.8}\text{Co}_{0.2}\text{Si}$  ( $T_C \sim 32$  K) ferromagnetic samples. For comparison, we have investigated the structural properties of  $\text{Fe}_{0.7}\text{Co}_{0.3}\text{Si}$  under pressure. Further information on the magnetic ground state of all three samples at ambient pressure was obtained using  $^{57}\text{Fe}$  Mössbauer-effect spectroscopy. We show that our investigations shed more insight into the nature of the ground state of  $\text{Fe}_{1-x}\text{Co}_x\text{Si}$  and provide a proper judge whether atomic disorder is responsible for the observed anomalous low-temperature behavior of the electrical resistivity at and beyond the critical pressure of the pressure-induced QPT.

## II. EXPERIMENT

All experiments presented here were carried out on high-quality single-phase polycrystalline  $\text{Fe}_{1-x}\text{Co}_x\text{Si}$  ( $x = 0.1, 0.2, 0.3$ ) samples. Details of the preparation of the samples are given elsewhere.<sup>4</sup>

To probe the temperature dependence of the electrical resistivity of  $\text{Fe}_{0.9}\text{Co}_{0.1}\text{Si}$  and  $\text{Fe}_{0.8}\text{Co}_{0.2}\text{Si}$  as a function of pressure, we performed high-pressure electrical resistivity measurements using a four-probe resistivity setup in a diamond anvil cell (DAC) made of a Ti-based alloy with a low expansion coefficient in order to minimize temperature-induced variations of the pressure. Gaskets were made of a mixture of Stycast 1266 and  $\text{Al}_2\text{O}_3$  (or BN). A typical sample chamber diameter was about  $200 \mu\text{m}$ . Measurements were done for temperatures  $1.6 \text{ K} \leq T \leq 300 \text{ K}$  using a  $^4\text{He}$  bath cryostat for pressures up to  $\sim 30$  GPa. In addition, we performed high-pressure magnetoresistance measurements at low temperatures ( $2 \text{ K} \lesssim T \lesssim 50 \text{ K}$ ) in external magnetic fields up to 8 T on  $\text{Fe}_{0.9}\text{Co}_{0.1}\text{Si}$  at 30 GPa using a  $^4\text{He}$  gas-flow cryostat with a superconducting magnet. Pressure was determined by the ruby fluorescence method<sup>29</sup> before and after each run.

To obtain information about the structural stability across the expected pressure-induced quantum phase transition, the pressure dependence of the structural parameters of the cubic lattice of  $\text{Fe}_{0.9}\text{Co}_{0.1}\text{Si}$ ,  $\text{Fe}_{0.8}\text{Co}_{0.2}\text{Si}$ , and  $\text{Fe}_{0.7}\text{Co}_{0.3}\text{Si}$  at room temperature up to 30.4 GPa, 23.1 GPa, and 9.0 GPa,

respectively, was determined by energy dispersive x-ray diffraction using synchrotron radiation at the beamline F3 at HASYLAB, Hamburg. Spectra were taken with  $E_{d_{hkl}} = 72.750 \text{ keV } \text{Å}$ ,  $E_{d_{hkl}} = 73.247 \text{ keV } \text{Å}$ , and  $E_{d_{hkl}} = 69.862 \text{ keV } \text{Å}$  for  $\text{Fe}_{0.9}\text{Co}_{0.1}\text{Si}$ ,  $\text{Fe}_{0.8}\text{Co}_{0.2}\text{Si}$ , and  $\text{Fe}_{0.7}\text{Co}_{0.3}\text{Si}$ , respectively, and a typical data acquisition time of 15–20 min. Pressure was generated in all cases by using a DAC setup with Bohler-Almax design type anvils<sup>30</sup> and Inconel 750 as gasket material. The diamonds had culets of 0.6 mm ( $\text{Fe}_{0.9}\text{Co}_{0.1}\text{Si}$  and  $\text{Fe}_{0.8}\text{Co}_{0.2}\text{Si}$ ) and 1.3 mm ( $\text{Fe}_{0.7}\text{Co}_{0.3}\text{Si}$ ). The applied pressure was determined either by the ruby fluorescence method or by using a tiny piece of gold inserted into the sample chamber. This allows one to determine the pressure *in situ* during acquisition of the spectrum via the calibrated lattice parameter of the cubic lattice of gold.<sup>31</sup> The obtained spectra were analyzed using the program EDXPOW.<sup>32</sup>

To investigate the magnetic ground state of  $\text{Fe}_{1-x}\text{Co}_x\text{Si}$  and its evolution with Co concentration  $x$  at a microscopic level, we have performed  $^{57}\text{Fe}$  Mössbauer spectroscopy measurements at ambient pressure and for temperatures  $4.2 \text{ K} \leq T \leq 300 \text{ K}$  for concentrations  $x = 0, 0.1, 0.2, 0.3$ . Using  $^{57}\text{Fe}$  Mössbauer spectroscopy, one is able to inspect the electronic and magnetic properties of systems containing Fe. Information about the valence state of Fe, local site symmetry, and the magnetic order and moment can be obtained from the isomer shift  $S$ , the quadrupole splitting  $QS$ , and the effective magnetic hyperfine field  $B_{\text{eff}}$  at the  $^{57}\text{Fe}$  nucleus, respectively. Since the  $\text{Fe}_{1-x}\text{Co}_x\text{Si}$  ( $0.1 \leq x \leq 0.3$ ) alloys are disordered samples, it is possible to observe a distribution of  $QS$  and  $B_{\text{eff}}$  which is expected to vary from site to site for the different samples.  $^{57}\text{Fe}$  Mössbauer spectra for  $\text{Fe}_{1-x}\text{Co}_x\text{Si}$  ( $x = 0.1, 0.2, 0.3$ ) were taken in a liquid  $^4\text{He}$  bath cryostat with a  $^{57}\text{Co}(\text{Rh})$  source and the absorber (sample) kept at the same temperature of 4.2 K. Sample thickness was about 10–15  $\text{mg}/\text{cm}^2$ . Additional spectra (not shown) were taken for all samples at room temperature and 90 K.

## III. RESULTS

### A. $^{57}\text{Fe}$ Mössbauer spectroscopy on $\text{Fe}_{1-x}\text{Co}_x\text{Si}$ at ambient pressure

Spectra have been taken at room temperature (RT), 90, and 4.2 K. The RT and 90-K spectra (not shown) all show a quadrupole line splitting  $QS$  due to a nonzero electric field gradient (EFG) at the  $^{57}\text{Fe}$  nucleus. They have been evaluated using a single enlarged quadrupole doublet and transmission integral. The results given in Table I (reference for isomer shift  $S$  is  $\alpha\text{-Fe}$  at room temperature) give the linewidth as the sum of the source and absorber values to better compare with literature values. These data are similar to those from Wertheim *et al.*<sup>33</sup> (Slight differences in average values are attributable to the different fit methods. Note differences in composition.)

The spectra from 4.2 K are shown in Fig. 1. It is known that, in nonmagnetic  $\text{FeSi}$ ,  $QS$  strongly depends on temperature for  $T$  above about 100 K but with little variation below.<sup>33</sup> The increased spectral broadening with Co content shown in Fig. 1 is a result of the magnetic order creating a magnetic hyperfine field  $B_{\text{eff}}$  at the  $^{57}\text{Fe}$  nucleus. This effect evidently increases over the composition range presented, similar to Wertheim

TABLE I. Results of  $^{57}\text{Fe}$  Mössbauer measurements of  $\text{Fe}_{1-x}\text{Co}_x\text{Si}$  ( $x = 0.1, 0.2, 0.3$ ) at room temperature (300 K), 90 K, and 4.2 K.  $\Gamma$ : linewidth;  $S$ : average isomer shift;  $QS$ : average quadrupole splitting;  $\overline{B}_{\text{eff}}$ : average hyperfine field;  $\sigma_x$ , ( $x = S, QS$ , and  $B$ ): standard deviations of  $S$ ,  $QS$ , and  $\overline{B}_{\text{eff}}$ . Typical errors are  $\pm 0.01$  mm/s and  $\pm 0.1$  T. Note that fits to the data at room temperature (300 K), 90 K, and for FeSi ( $x = 0$ ) at 4.2 K are single-site fits using the transmission integral.

	$x$			
	0	0.1	0.2	0.3
300 K				
$\Gamma$ (mm/s)	0.25	0.24	0.27	0.26
$S$ (mm/s)	0.25	0.26	0.26	0.26
$QS$ (mm/s)	0.50	0.51	0.50	0.50
90 K				
$\Gamma$ (mm/s)	0.32		0.31	0.32
$S$ (mm/s)	0.35		0.35	0.36
$QS$ (mm/s)	0.72		0.62	0.60
4.2 K				
$\Gamma$ (mm/s)	0.25	0.25	0.25	0.25
$S$ (mm/s)	0.39	0.40	0.41	0.41
$\sigma_S$ (mm/s)		0.00	0.01	0.00
$QS$ (mm/s)	0.74	0.70	0.63	0.59
$\sigma_{QS}$ (mm/s)		0.00	0.07	0.08
$\overline{B}_{\text{eff}}$ (T)	0.0	0.82	1.7	2.5
$\sigma_B$ (T)		0.94	1.4	1.4

*et al.*<sup>33</sup> However, the magnetic splitting of the nuclear sublevels is not large compared to the effect of the EFG, necessitating the use of the full Hamiltonian for  $^{57}\text{Fe}$  with mixed EFG and  $B_{\text{eff}}$  interactions. The line positions and intensities then depend on the relative orientation between the EFG principal axis and  $B_{\text{eff}}$ . From the crystal structure of FeSi, the EFG principal axis at the iron site is along  $\langle 111 \rangle$  directions and the asymmetry parameter is zero.<sup>35</sup> At low Co concentration, the iron moments are along  $\langle 100 \rangle$  directions but become random with increasing Co concentration.<sup>10</sup> Since the four possible  $\langle 111 \rangle$  directions are all at an angle of  $\arccos(1/\sqrt{3})$  to  $\langle 100 \rangle$ , diagonal EFG terms drop out of the Hamiltonian, but nondiagonal terms do not (see, for example, Ref. 34).

In order to exploit the spectra from 4.2 K, first they were fit using the transmission integral and the full Hamiltonian with the fixed angle  $\arccos(1/\sqrt{3})$  to  $\langle 100 \rangle$  between the EFG principal axis and  $B_{\text{eff}}$ . Then they were also fit assuming an isotropic distribution between the EFG principal axis and  $B_{\text{eff}}$ . An expression for the angular-averaged (isotropic) case for fixed  $QS$  and  $B_{\text{eff}}$  has been given by Blaes *et al.*<sup>34</sup> These two methods yield about the same values of  $S$ ,  $QS$ , and  $B_{\text{eff}}$ . However, these fits were far from adequate. This shows that the dispersion in  $B_{\text{eff}}$  is too large to be simply included in an enlarged linewidth. In order to compensate for this magnetic distribution, we were obliged to use a histogram routine. However the single-site transmission-integral fits were used as a guide for the following fits. It was also necessary to use a routine which starts from the full Hamiltonian for mixed hyperfine interactions. Since the single-site results indicated little difference for the three fits between a fixed (single-site

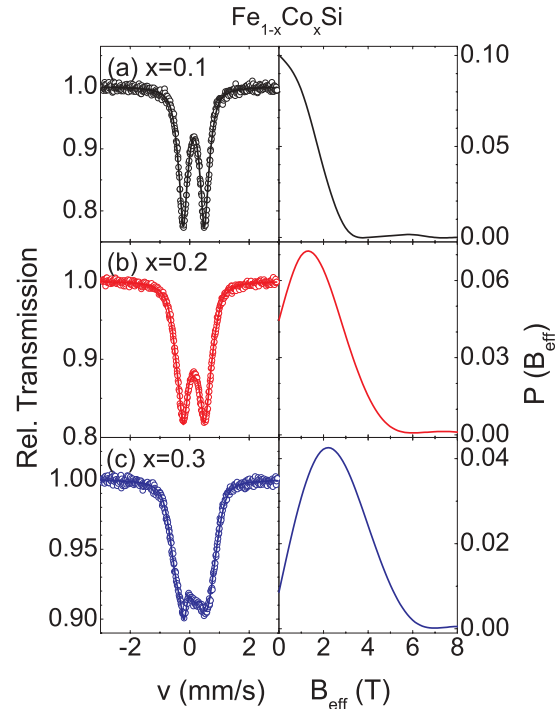


FIG. 1. (Color online) Left panel: Mössbauer spectra of  $\text{Fe}_{1-x}\text{Co}_x\text{Si}$  ( $x = 0.1, 0.2, 0.3$ ) at 4.2 K. Solid line corresponds to the histogram fit of the data involving a distribution of  $B_{\text{eff}}$  including mixed hyperfine interactions using the Blaes *et al.* routine.<sup>34</sup> Small linear variations of center shift  $S$  and quadrupole splitting  $QS$  were allowed. Right panel:  $B_{\text{eff}}$  distribution  $P(B_{\text{eff}})$  obtained from fitting the spectra at 4.2 K.

Hamiltonian) and an isotropic (Blaes *et al.*) distribution, the Blaes *et al.* routine was used in the following.

The spectra for  $x = 0.1, 0.2, 0.3$  were fit using a histogram of subspectra at fixed  $B_{\text{eff}}$  values. The histogram routine calculates the distribution  $P(QS)$  or  $P(B_{\text{eff}})$  but obliges the use of the thin-absorber approximation. The results given for 90 K in Table I show that  $QS$  decreases slightly with increasing Co content. Thus, a criterion to judge the distribution fits was that this tendency should be obtained as well. They were fit using a series of subspectra at intervals of 1 T, allowing the center shift and  $QS$  to vary. In addition, linear variations of both  $S$  and  $QS$  were allowed whereby only small resulting variations are taken as physically relevant. A small smoothing-parameter constraint as well as small constraints on initial and final values of  $P(B_{\text{eff}})$  were assumed. But variation of these constraints lead to only small changes in the average values and standard deviations reported on below.

The theoretical fits are given in Fig. 1 (obtained by WinNormos<sup>36</sup>). The left panel gives the spectra and fitted curve, while the right panel shows the three distributions  $P(B_{\text{eff}})$ . Calculating  $P(B_{\text{eff}})$  from the spectra we obtain the average values of  $S$ ,  $QS$ , and  $B_{\text{eff}}$ . To characterize the width of the distribution, the standard deviations  $\sigma_x$  ( $x = S, QS, \overline{B}_{\text{eff}}$ ) have been calculated as well and are given in the table for these spectra. Essentially no dispersion was found in  $S$  or  $QS$ . The results yield the histogram of  $B_{\text{eff}}$ . The average values as well as the standard deviations are presented in Table I (reference for  $S$  is  $\alpha$ -Fe at room temperature).

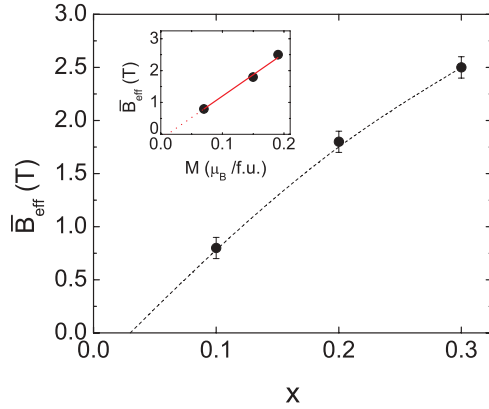


FIG. 2. (Color online) Average magnetic hyperfine field  $\bar{B}_{\text{eff}}$  of  $\text{Fe}_{1-x}\text{Co}_x\text{Si}$  as a function of concentration  $x$ . Dotted line is only a guide to the eye. The inset shows that  $\bar{B}_{\text{eff}}$  is proportional to the magnetization  $M$  obtained by macroscopic measurements. The values of  $M$  are taken from Ref. 5. The solid red line is a linear fit to the data, the dotted part is an extrapolation of this linear fit toward zero field.

The concentration dependence of the average magnetic hyperfine field  $\bar{B}_{\text{eff}}$  is shown in Fig. 2.  $\bar{B}_{\text{eff}}$  nearly reveals a linear increase with increasing concentration and roughly indicates that the onset of magnetic order is between 0.02 and 0.05, close to what has been reported from magnetization measurements.<sup>4,5</sup> Also, the inset of Fig. 2 displays a good correlation between  $\bar{B}_{\text{eff}}$  and the value of the magnetic moment; that is,  $\bar{B}_{\text{eff}}$  exhibits the same concentration dependence as the magnetic moment.

### B. Pressure dependence of the electrical resistivity

The temperature dependence ( $1.6 \text{ K} \leq T \leq 300 \text{ K}$ ) of the electrical resistivity  $\rho(T, p)$  of  $\text{Fe}_{0.9}\text{Co}_{0.1}\text{Si}$  for different pressures from ambient pressure up to 29.9 GPa is shown in Fig. 3(a). The resistivity at ambient pressure first increases rapidly with decreasing temperature, reaches a broad maximum around  $T_{\text{max}} \sim 65 \text{ K}$ , and then decreases. At low temperatures, the resistivity shows a weak upturn at  $T_{\text{M}} \sim 11 \text{ K}$ , which is due to the onset of ferromagnetic order below  $T_{\text{C}}$ . Thus,  $T_{\text{max}}$  can be identified as the temperature below which the system becomes metallic. The observed features are in full agreement with those reported for  $\text{Fe}_{0.7}\text{Co}_{0.3}\text{Si}$ .<sup>5</sup> Upon increasing the pressure, the maximum is gradually shifted to higher temperatures, and the upturn of the resistivity at  $T_{\text{M}}$  disappears, suggesting that magnetic order is suppressed (at least down to 1.6 K); that is, a pressure-induced quantum phase transition (QPT) is observed.

Figure 3(b) shows the temperature dependence ( $1.6 \text{ K} \leq T \leq 300 \text{ K}$ ) of the electrical resistivity of  $\text{Fe}_{0.8}\text{Co}_{0.2}\text{Si}$  for different pressures from ambient pressure up to  $p = 15.3 \text{ GPa}$ . As is evident from the figure, one observes a similar type of behavior for  $\rho(T, p)$  with increasing pressure as for  $\text{Fe}_{0.9}\text{Co}_{0.1}\text{Si}$ . However, the maximum in  $\rho(T)$  appears in this sample at a higher temperature ( $T_{\text{max}} \sim 110 \text{ K}$ ). In addition, due to the higher value of  $T_{\text{C}} \sim 32 \text{ K}$ , one clearly observes a pressure-induced shift of the resistivity upturn at  $T_{\text{M}}$  to lower temperatures which nearly disappears above  $\sim 11 \text{ GPa}$ . This

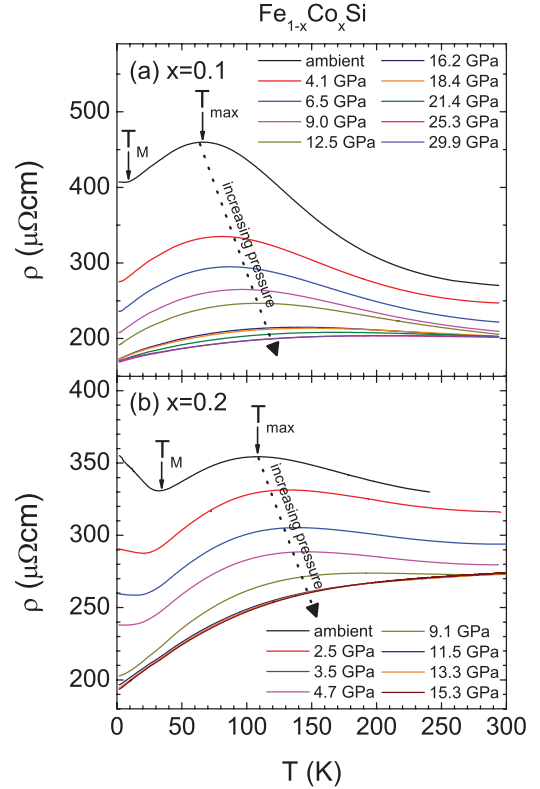


FIG. 3. (Color online) Temperature dependence of the resistivity of (a)  $\text{Fe}_{0.9}\text{Co}_{0.1}\text{Si}$  and (b)  $\text{Fe}_{0.8}\text{Co}_{0.2}\text{Si}$  for different pressures from ambient pressure up to 29.9 and 15.3 GPa, respectively, as obtained by four-point electrical resistivity measurements using a diamond anvil cell setup. The arrows at ambient pressure indicate the maxima in  $\rho(T)$  at  $T_{\text{max}}$ , below which the systems show a metallic-like temperature dependence of  $\rho(T)$ , and the anomalies at  $T_{\text{M}}$  which are connected with the onset of ferromagnetic order in  $\text{Fe}_{0.9}\text{Co}_{0.1}\text{Si}$  ( $T_{\text{C}} \sim 11 \text{ K}$ ) and  $\text{Fe}_{0.8}\text{Co}_{0.2}\text{Si}$  ( $T_{\text{C}} \sim 32 \text{ K}$ ).<sup>5</sup>

again suggests a pressure-induced magnetic quantum phase transition in  $\text{Fe}_{0.8}\text{Co}_{0.2}\text{Si}$ .

The evolution of  $\rho(T, p)$  with pressure in both samples can be qualitatively explained on the basis of the electronic structure of the undoped FeSi sample assuming two narrow bands with a high density of states and the Fermi energy  $E_{\text{F}}$  lying in the gap between the two bands.<sup>11,37</sup> Obviously, upon electron doping, impurity or defect states and the associated mobility edge result in a finite density of states at  $E_{\text{F}}$ . As a consequence,  $\rho(T)$  exhibits a metallic-like behavior at low temperatures. This, however, changes to a semiconducting-like behavior above  $T_{\text{max}}$  due to a considerable thermal activation of the charge carriers across the energy gap between the two narrow bands. Since external pressure is expected to cause a broadening of the bands, the density of states at  $E_{\text{F}}$  will gradually decrease with pressure. Simultaneously, the energy gap will decrease due to the broadening of the bands. Thus, a metallic state is stabilized at higher temperature. As a result,  $T_{\text{max}}$  is gradually shifted toward higher temperatures with increasing pressure and a metallic behavior is achieved in the whole temperature range for  $p \gtrsim 25 \text{ GPa}$  and  $p \gtrsim 11 \text{ GPa}$  for  $\text{Fe}_{0.9}\text{Co}_{0.1}\text{Si}$  and  $\text{Fe}_{0.8}\text{Co}_{0.2}\text{Si}$ , respectively. Thus,  $T_{\text{max}}$  represents the energy scale for the transition from the

metallic to the insulating state upon increasing temperature. Bearing in mind that ferromagnetism in such a band (itinerant) picture originates from the difference (shift) between the majority (spin-up) and minority (spin-down)  $3d$  bands at the Fermi level, the observed pressure-induced suppression of the ferromagnetic state can simply be explained by a gradual decrease of the splitting between spin-up and spin-down bands. It should be mentioned that the band picture discussed above is consistent with band structure calculations for  $\text{Fe}_{1-x}\text{Co}_x\text{Si}$ .<sup>6</sup>

### C. Pressure dependence of the crystal structure

The spectra of  $\text{Fe}_{1-x}\text{Co}_x\text{Si}$  ( $x = 0.1, 0.2, 0.3$ ) recorded at room temperature for different pressures are shown in Figs. 4(a)–4(c). All Bragg reflections from the samples can be indexed according to the B20 structure; a structural phase transition is not observed within the experimental accuracy for all samples in the inspected pressure range.

Additional reflections are observed in the spectra of  $\text{Fe}_{0.8}\text{Co}_{0.2}\text{Si}$  [Fig. 4(b)] and  $\text{Fe}_{0.7}\text{Co}_{0.3}\text{Si}$  [Fig. 4(c)], which originate from the gold pressure marker [asterisks in Fig. 4(b,c)]. For  $\text{Fe}_{0.8}\text{Co}_{0.2}\text{Si}$ , one intense peak appears at  $\sim 5.2$  keV, which is pressure independent. Thus, it originates not from a different phase but is due to a scattering event outside the sample chamber or caused by a problem in the detector. As shown for  $\text{Fe}_{0.7}\text{Co}_{0.3}\text{Si}$  in Fig. 4(c), the appearance of new reflections observed for  $p \sim 5$  GPa can be assigned to the cubic phase of solidified nitrogen. It is known that solid nitrogen undergoes a phase transition from a hexagonal phase ( $P6_3/mmc$ ) to a primitive cubic phase ( $Pm\bar{3}n$ ) at this pressure at room temperature.<sup>38</sup>

The lattice parameter  $a$  of the cubic unit cell of all  $\text{Fe}_{1-x}\text{Co}_x\text{Si}$  samples was determined by using the (110), (111), (210), (211), and (321) reflections. As can be seen in the insets of Figs. 5(a)–5(c), the lattice parameter  $a$  of all samples is reduced smoothly with increasing pressure, indicating no evidence for a structural phase transition. The values of  $a$  at ambient pressure are 4.48 (2) Å, 4.47, (2) Å, and 4.47 (2) Å for the samples with  $x = 0.1, x = 0.2$ , and  $x = 0.3$ , respectively. The pressure dependence of the volume of the unit cell  $V = a^3$  shown in Figs. 5(a)–5(c) can be approximated by the Murnaghan equation of state.<sup>39</sup> The derived values of the bulk modulus  $B_0$  and its derivative with pressure  $B'_0$  are  $B_0 = 178$  (5) GPa, 190 (4) GPa, and 197 (11) GPa and  $B'_0 = 4.7$  (4), 4.7 (fixed), and 3 (2), for  $x = 0.1, 0.2$ , and 0.3, respectively. There is a slight stiffening upon increasing Co doping.

## IV. DISCUSSION

### A. Quantum phase transition in $\text{Fe}_{0.9}\text{Co}_{0.1}\text{Si}$ under pressure

As already mentioned in Sec. III B, the pressure dependence of  $\rho(T, p)$  suggests a pressure-induced magnetic to nonmagnetic transition in  $\text{Fe}_{0.9}\text{Co}_{0.1}\text{Si}$  and  $\text{Fe}_{0.8}\text{Co}_{0.2}\text{Si}$ . In this section we first focus on the analysis of the pressure dependence of  $T_M$  and the nature of the high-pressure nonmagnetic state in the nearly ordered  $\text{Fe}_{0.9}\text{Co}_{0.1}\text{Si}$  sample (section IV A and IV B, respectively). We then compare the pressure dependence of  $T_M$  in all samples ( $x = 0.1, 0.2, 0.3$ ) in Sec. IV C and finally

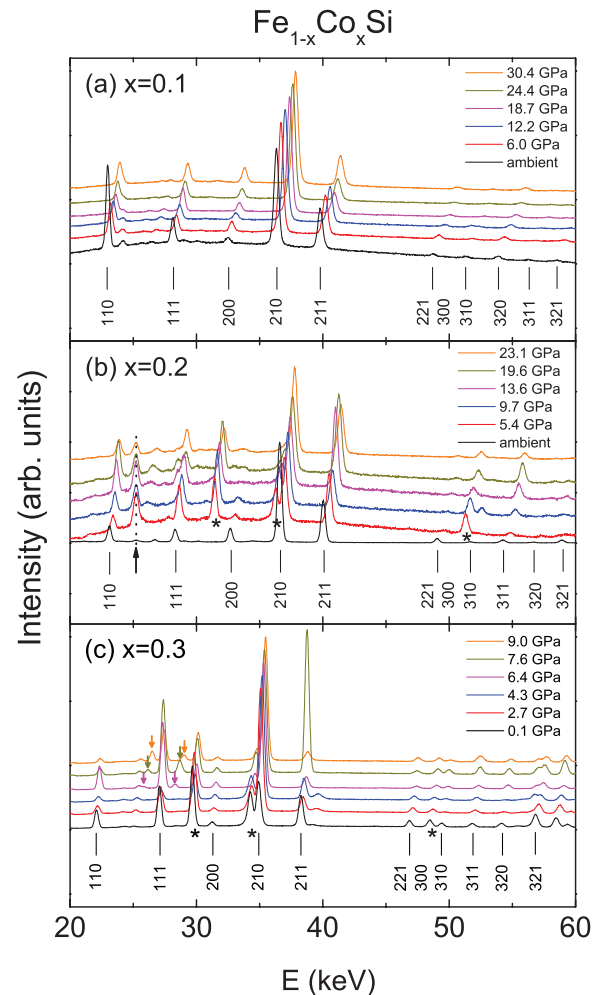


FIG. 4. (Color online) X-ray diffraction patterns of  $\text{Fe}_{1-x}\text{Co}_x\text{Si}$  ( $x = 0.1, 0.2, 0.3$ ) at room temperature as obtained from energy dispersive x-ray diffraction at beamline F3 (HASYLAB, Hamburg) using a diamond anvil cell setup. (a) Patterns of  $\text{Fe}_{0.9}\text{Co}_{0.1}\text{Si}$  for selected pressures up to 30 GPa recorded with  $E_{d_{hkl}} = 72.750$  keV Å. (b) Patterns of  $\text{Fe}_{0.8}\text{Co}_{0.2}\text{Si}$  for selected pressures up to 23.1 GPa recorded with  $E_{d_{hkl}} = 73.247$  keV Å. The arrow marks the peak from the detector electronics, which remains pressure independent as demonstrated by the dotted line. The asterisks mark the peaks from the gold pressure marker. (c) Patterns of  $\text{Fe}_{0.7}\text{Co}_{0.3}\text{Si}$  for selected pressures up to 9.0 GPa recorded with  $E_{d_{hkl}} = 69.862$  keV Å. The arrows mark the peaks from solid nitrogen in the cubic phase above  $p \sim 5$  GPa, the asterisks mark the peaks from the gold pressure marker. The high intensity of the peak at about 37 keV for 7.6 GPa results from the texture of the sample and is not observed at other pressures.

discuss the origin of the stability of the ferromagnetic state in Sec. IV D.

To understand the nature of the pressure-induced quantum phase transition in the  $\text{Fe}_{0.9}\text{Co}_{0.1}\text{Si}$  sample, we now consider the temperature dependence of  $\rho(T, p)$  in the low-temperature region below 20 K. The resistivity normalized to its value at 20 K [ $\rho(T)/\rho(20\text{ K})$ ] for  $\text{Fe}_{0.9}\text{Co}_{0.1}\text{Si}$  is shown in Fig. 6 for  $1.6\text{ K} \leq T \leq 20\text{ K}$  from ambient pressure to  $p = 9.0$  GPa. As can be seen in Fig. 6, the temperature coefficient  $\alpha_\rho = \partial\rho/\partial T$  is positive, reflecting a metallic ground state of  $\text{Fe}_{0.9}\text{Co}_{0.1}\text{Si}$ ,

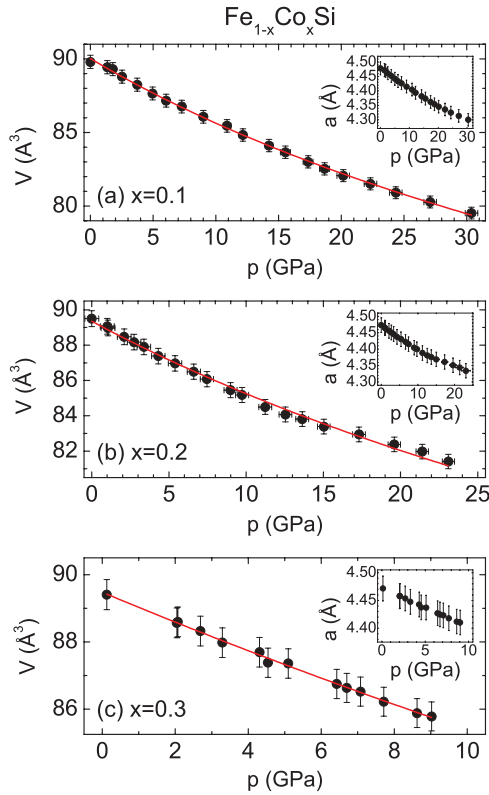


FIG. 5. (Color online) Pressure dependence of the volume  $V$  of the cubic unit cell at room temperature of (a)  $\text{Fe}_{0.9}\text{Co}_{0.1}\text{Si}$  up to 30.4 GPa, (b)  $\text{Fe}_{0.8}\text{Co}_{0.2}\text{Si}$  up to 23.1 GPa, and (c)  $\text{Fe}_{0.7}\text{Co}_{0.3}\text{Si}$  up to 9.0 GPa. Red lines are fits to the data using the Murnaghan equation of state (see text). The insets show the pressure dependence of the corresponding  $a$  axis of  $\text{Fe}_{1-x}\text{Co}_x\text{Si}$  ( $x = 0.1, 0.2, 0.3$ ).

but changes drastically upon applying pressure. The values of  $T_M$  at different pressures have been determined by the upturn or kink where the temperature dependence of  $\rho(T, p)$  deviates from the linear behavior found at higher temperatures. Using this criterion, we obtain a value of  $\sim 11$  K (see Fig. 6),

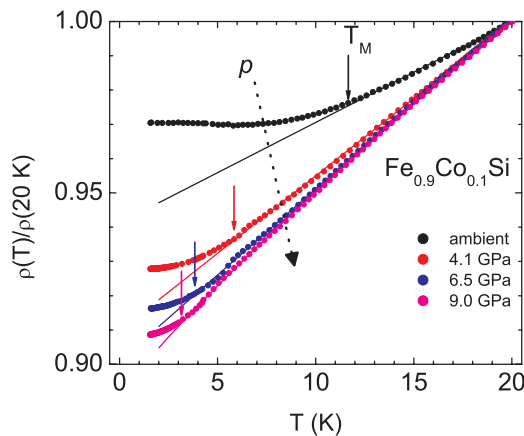


FIG. 6. (Color online) Temperature dependence of the normalized electrical resistivity  $\rho(T)/\rho(20\text{ K})$  of  $\text{Fe}_{0.9}\text{Co}_{0.1}\text{Si}$  in the low-temperature region ( $1.6\text{ K} \leq T \leq 20\text{ K}$ ) for different pressures from ambient pressure up to  $p = 9.0$  GPa. Arrows mark  $T_M$ , which is connected with the onset of magnetic ordering.

which is in a very good agreement with that reported from magnetization measurements.<sup>5</sup> As is evident from Fig. 6,  $T_M$  is gradually suppressed to  $T_M < 1.6$  K at 12.5 GPa, indicating a nonmagnetic metallic state for  $p \geq 12.5$  GPa. For  $12.5\text{ GPa} \leq p \leq 29.9$  GPa no anomaly, which can be attributed to the onset of an ordering phenomenon, is observed. Thus, there is no indication for a further change of the ground-state properties in this pressure region.

### B. Nature of the nonmagnetic metallic high-pressure state of $\text{Fe}_{0.9}\text{Co}_{0.1}\text{Si}$

In this section, we first discuss the nature of the nonmagnetic metallic state of the less disordered sample  $\text{Fe}_{0.9}\text{Co}_{0.1}\text{Si}$  at high pressure and then compare it with those observed in  $\text{Fe}_{0.7}\text{Co}_{0.3}\text{Si}$  and in relevant systems such as  $\text{MnSi}$  and  $\text{FeGe}$ . The observed pressure-induced suppression of the magnetic order in  $\text{Fe}_{0.9}\text{Co}_{0.1}\text{Si}$  is remarkably similar to that reported for  $\text{Fe}_{0.7}\text{Co}_{0.3}\text{Si}$ ,<sup>5</sup>  $\text{MnSi}$ ,<sup>25</sup> and  $\text{FeGe}$ .<sup>28</sup> To quantitatively describe the temperature dependence in the nonmagnetic metallic high-pressure phase of  $\text{Fe}_{0.9}\text{Co}_{0.1}\text{Si}$ , a power law of the form  $\rho(T) \propto AT^n$  was applied to the resistivity data in the temperature range  $1.6\text{ K} \leq T \leq 20\text{ K}$ . The product  $AT^n$  accounts for electron-magnon coupling and/or electron-electron scattering.<sup>28</sup> Since it is not adequate to use a power law in the magnetically ordered state, we only show in Fig. 7 the pressure dependence of the coefficient  $A$  and the exponent  $n$  in the nonmagnetic metallic state for  $p \geq 12.5$  GPa. As shown in the figure, the coefficient  $A$  decreases sharply for  $12.5\text{ GPa} \leq p \leq 25.3$  GPa from  $A = 1.36\ \mu\Omega\text{ cm}^{-1}\text{ K}^{-n}$  to  $A = 0.54\ \mu\Omega\text{ cm}^{-1}\text{ K}^{-n}$  for 12.5 GPa and 25.3 GPa, respectively. In contrast, the value of the exponent  $n$  is found to be nearly pressure independent from 12.5 to 29.9 GPa at a value  $n \sim 1$ . This means that at or near the QPT, and also far above  $p_c$ , the electrical resistivity of  $\text{Fe}_{0.9}\text{Co}_{0.1}\text{Si}$  is proportional to the temperature [i.e.,  $\rho(T) \propto T$ ]. We note that such an unusual exponent ( $n \sim 1$ ) has been

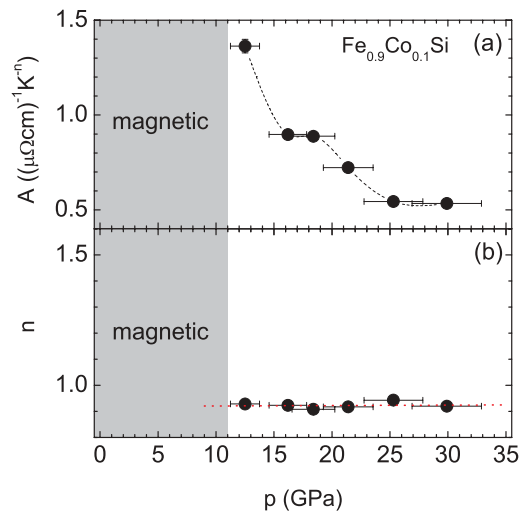


FIG. 7. (Color online) Pressure dependence of (a) the coefficient  $A$  and (b) the exponent  $n$  as obtained from the temperature dependence of the electrical resistivity ( $\rho = \rho_0 + AT^n$ ) in the nonmagnetic metallic state of  $\text{Fe}_{0.9}\text{Co}_{0.1}\text{Si}$  for  $p \geq 12.5$  GPa. The dark areas mark the region where magnetic order exists.

also observed for  $\text{Fe}_{0.7}\text{Co}_{0.3}\text{Si}$  in the nonmagnetic metallic state and is indicative of non-Fermi liquid behavior.<sup>5</sup>

The enhancement of  $A$  close to the QPT in  $\text{Fe}_{0.9}\text{Co}_{0.1}\text{Si}$  is also found for both MnSi and FeGe.<sup>28</sup> The high-pressure non-Fermi liquid regime in  $\text{Fe}_{0.9}\text{Co}_{0.1}\text{Si}$  persists up to pressures of at least  $p \sim 2.5p_c$ , which is much higher than the critical pressure where the QPT is located. A similar observation has been reported in MnSi, where the non-Fermi liquid behavior also survives up to much higher pressures than the critical pressure ( $p \sim 3p_c$ ).<sup>26,27</sup> However, the unusual temperature dependence of the electrical resistivity [ $\rho(T) \propto T$ ] found in  $\text{Fe}_{1-x}\text{Co}_x\text{Si}$  for  $p \gtrsim p_c$  for  $x = 0.1$  and  $x = 0.3$  is clearly distinct from the temperature dependence found both in MnSi and FeGe [ $\rho(T) \propto T^{1.5}$ ] at low temperatures at or near the QPT<sup>28,40</sup> and also different from what one would expect from the Hertz-Moriya-Millis spin fluctuation scenario.<sup>41–43</sup> This points to a considerable difference in the nature of the high-pressure ground states of the  $\text{Fe}_{1-x}\text{Co}_x\text{Si}$  system and MnSi or FeGe. It has been proposed that disorder might be the reason for the unusual temperature dependence of  $\rho(T)$  found for  $\text{Fe}_{0.7}\text{Co}_{0.3}\text{Si}$ .<sup>5</sup> However, since this temperature dependence is also found in nearly ordered  $\text{Fe}_{0.9}\text{Co}_{0.1}\text{Si}$ , the observed non-Fermi liquid behavior and its unusual exponent  $n$  is found to be independent on the degree of disorder and seems to be an intrinsic property of  $\text{Fe}_{1-x}\text{Co}_x\text{Si}$ .

Further information on the high-pressure nonmagnetic state of  $\text{Fe}_{0.9}\text{Co}_{0.1}\text{Si}$  is provided from the investigation of the electrical resistivity in external magnetic fields [magnetoresistance (MR)]. Figure 8 shows measurements of the electrical resistivity of  $\text{Fe}_{0.9}\text{Co}_{0.1}\text{Si}$  at  $p = 30$  GPa in external magnetic fields  $0 \text{ T} \leq B \leq 8 \text{ T}$ . As can be seen, the electrical resistivity increases at 2 K from  $\rho_{2\text{K}} = 169.6 \mu\Omega\text{cm}$  in zero field to about  $\rho_{2\text{K}} = 173.4 \mu\Omega\text{cm}$  ( $\sim 2.2\%$ ) in an external field of 8 T. A positive magnetoresistance is also observed in the same compound at ambient pressure.<sup>4,5</sup> However, the size of the magnetoresistance MR at 2.5 K and 8 T is significantly

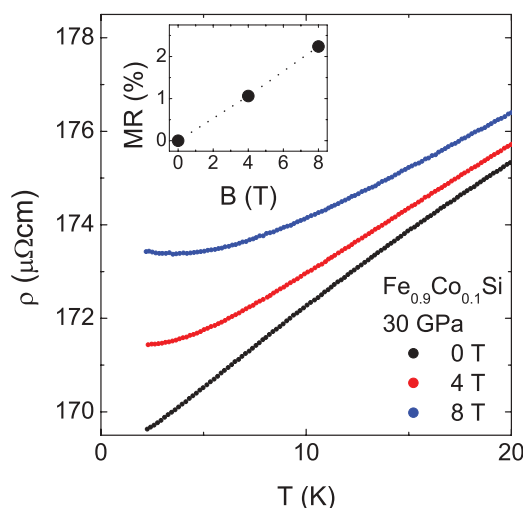


FIG. 8. (Color online) Temperature dependence of the electrical resistivity of  $\text{Fe}_{0.9}\text{Co}_{0.1}\text{Si}$  at 30 GPa for  $T \leq 20$  K in external magnetic fields up to 8 T. The inset shows the magnetoresistance MR at 2.5 K in percent as a function of external magnetic field for  $\text{Fe}_{0.9}\text{Co}_{0.1}\text{Si}$  at 30 GPa (see text).

reduced from MR  $\sim 10\%$  at ambient pressure to MR  $\sim 2.2\%$  for  $p = 30$  GPa (see inset in Fig. 8).

The observation of a positive MR in the nonmagnetic state indicates that the band picture drawn by Onose *et al.*<sup>5</sup> is appropriate to describe the underlying physics of the unusual sign of the MR. Assuming a Stoner-type weak itinerant ferromagnetism, it is argued<sup>5</sup> that an external magnetic field depopulates the spin minority band, which is found to be much more mobile than the majority band and, thus, results in a higher resistivity.<sup>5,44</sup> The finding of a pressure-induced nonmagnetic ground state, which exhibits a positive MR in the present study, can now be explained, if one assumes that an external magnetic field leads to a small imbalance between the population of the majority and minority spin bands (i.e., a very small ferromagnetic moment) and, thereby, to the observed small positive MR. This further demonstrates the entire difference of the nature of the high-pressure states of  $\text{Fe}_{1-x}\text{Co}_x\text{Si}$  and MnSi.

### C. Comparison of the pressure dependence of $T_M$ in $\text{Fe}_{1-x}\text{Co}_x\text{Si}$

We now turn to the analysis of the pressure dependence of the upturn or kink in  $\text{Fe}_{1-x}\text{Co}_x\text{Si}$  with  $x = 0.2$  and then compare the obtained data with those of  $x = 0.1$  and 0.3. Figure 9(a) shows the normalized resistivity  $\rho(T)/\rho(60 \text{ K})$  of  $\text{Fe}_{0.8}\text{Co}_{0.2}\text{Si}$  as a function of temperature for  $T \leq 60$  K and  $p \leq 4.7$  GPa. In this pressure regime, the temperature coefficient  $\alpha_\rho$  is negative at low temperatures and approaches

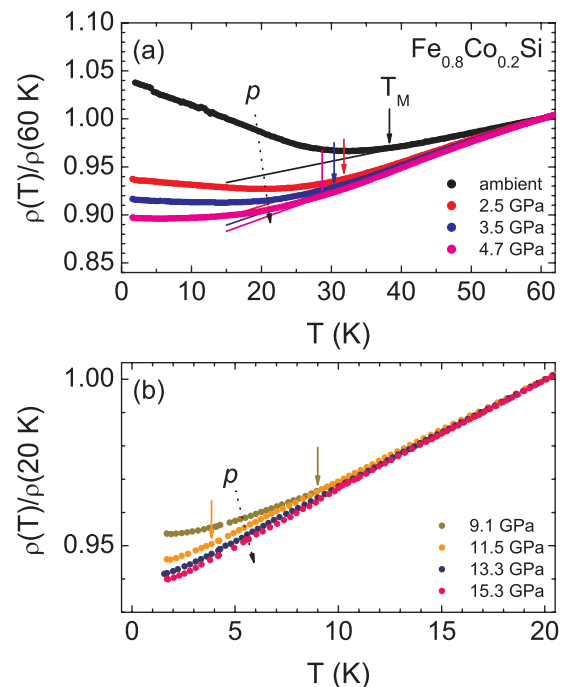


FIG. 9. (Color online) Temperature dependence of the normalized electrical resistivity  $\rho(T)/\rho(60 \text{ K})$  of  $\text{Fe}_{0.8}\text{Co}_{0.2}\text{Si}$  for  $1.6 \text{ K} \leq T \leq 60 \text{ K}$  for different pressures from ambient pressure up to  $p = 9.1$  GPa. Arrows mark  $T_M$ , which is connected with the onset of magnetic ordering. (b) Temperature dependence of the normalized electrical resistivity  $\rho(T)/\rho(20 \text{ K})$  of  $\text{Fe}_{0.8}\text{Co}_{0.2}\text{Si}$  for  $1.6 \text{ K} \leq T \leq 20 \text{ K}$  for different pressures in the range  $11.5 \text{ GPa} \leq p \leq 15.3 \text{ GPa}$ .

zero as  $p \rightarrow 4.7$  GPa. As indicated by the arrows, an upturn or kink at  $T_M$  is visible where ferromagnetic ordering sets in ( $T_C \sim 32$  K at ambient pressure). For pressures above 9.1 GPa,  $\alpha_\rho$  becomes positive, indicating a further suppression of the magnetism as can be seen in Fig. 9(b), which displays the temperature dependence of the normalized resistivity  $\rho(T)/\rho(20$  K) for  $T \leq 20$  K and  $9.1$  GPa  $\leq p \leq 15.3$  GPa. A clear sign of  $T_M$  cannot be tracked anymore for  $p > 11.5$  GPa. However, the ratio  $\rho(1.6$  K)/ $\rho(20$  K) further decreases with increasing pressure up to  $p = 15.3$  GPa. It should be noted here that the signature of  $T_M$  in  $\text{Fe}_{0.8}\text{Co}_{0.2}\text{Si}$  is much less pronounced than in  $\text{Fe}_{0.9}\text{Co}_{0.1}\text{Si}$ . This can be an intrinsic property of the sample possibly due to the fact that  $\text{Fe}_{0.8}\text{Co}_{0.2}\text{Si}$  is expected to exhibit more disorder than  $\text{Fe}_{0.9}\text{Co}_{0.1}\text{Si}$ . It can also be due to large pressure gradients and/or nonhydrostatic conditions in this particular high-pressure run.

Based on the analysis given above, a comparison of the pressure dependence of  $T_M$  which is connected to the onset of ferromagnetic order in all three  $\text{Fe}_{1-x}\text{Co}_x\text{Si}$  ( $x = 0.1, 0.2, 0.3$ ) samples is presented in Fig. 10. Following the pressure dependence of  $T_M$ , the magnetic order in  $\text{Fe}_{0.9}\text{Co}_{0.1}\text{Si}$  is suppressed with increasing pressure with  $\partial T_M/\partial p \sim -1.0$  K/GPa from  $\sim 11$  K at ambient pressure to  $\sim 3.2$  K at 9.0 GPa. Extrapolation of the pressure dependence to  $T \rightarrow 0$  yields a critical pressure of  $p_c \sim 11$  GPa. In the case of  $\text{Fe}_{0.8}\text{Co}_{0.2}\text{Si}$ ,  $T_M$  decreases with increasing pressure from  $\sim 39$  K at ambient pressure to  $\sim 4$  K at 11.5 GPa. Above this pressure, there is no clear kink observed for a possible onset of magnetic order. Assuming a linear pressure dependence of  $T_M$  for  $p \leq 11.5$  GPa, one obtains  $\partial T_M/\partial p \sim -3.2$  K/GPa. Extrapolation to zero temperature gives a critical pressure of  $p_c \sim 12.2$  GPa. According to Ref. 5,  $T_M$  of  $\text{Fe}_{0.7}\text{Co}_{0.3}\text{Si}$ , decreases from 51 K at ambient pressure toward zero temperature with  $\partial T_M/\partial p \sim -7.1$  K/GPa which results in a critical pressure of  $p_c \sim 7$  GPa.

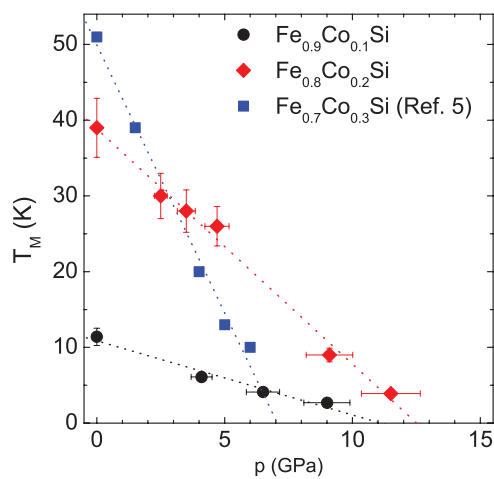


FIG. 10. (Color online) Pressure dependence of the upturn or kink at  $T_M$  of the electrical resistivity at low temperatures, which is connected to the onset of magnetic order in  $\text{Fe}_{1-x}\text{Co}_x\text{Si}$  ( $x = 0.1, 0.2, 0.3$ ). The data points of  $\text{Fe}_{0.9}\text{Co}_{0.1}\text{Si}$  and  $\text{Fe}_{0.8}\text{Co}_{0.2}\text{Si}$  were obtained in this study whereas the data points of  $\text{Fe}_{0.7}\text{Co}_{0.3}\text{Si}$  were reported by Onose *et al.* (Ref. 5). Dotted lines are linear fits to the experimental data points.

If one would assume that the magnetic structure of  $\text{Fe}_{1-x}\text{Co}_x\text{Si}$  does not change with Co concentration  $x$ , the observed systematic increasing pressure dependence of  $T_M$  with increasing  $x$  is unexpected. This is due to the fact that both the spontaneous magnetic moment  $\mu_{\text{Fe}}$  and thereby the magnetic ordering temperature  $T_C$  increase with increasing  $x$ , reflecting a systematic strengthening of the ferromagnetism when going from  $\text{Fe}_{0.9}\text{Co}_{0.1}\text{Si}$  through  $\text{Fe}_{0.8}\text{Co}_{0.2}\text{Si}$  ( $\mu_{\text{Fe}} \sim 0.15 \mu_B$ ,  $T_C \sim 32$  K) to  $\text{Fe}_{0.7}\text{Co}_{0.3}\text{Si}$  ( $\mu_{\text{Fe}} \sim 0.20 \mu_B$ ,  $T_C \sim 43$  K). In other words, the stronger ferromagnetic state in  $\text{Fe}_{0.7}\text{Co}_{0.3}\text{Si}$  is more sensitive to pressure than the weaker one of  $\text{Fe}_{0.9}\text{Co}_{0.1}\text{Si}$ . To explain the origin of such an unexpected behavior, other factors that can affect the stability of the ferromagnetic state in the system under high pressure will be discussed in Sec. IV D.

#### D. Origin of the stability of the ferromagnetic state under high pressure

In the following, we try to provide an explanation of the observed pressure dependence of  $T_M$  in the  $\text{Fe}_{1-x}\text{Co}_x\text{Si}$  samples, which shows a systematic increase with increasing Co concentration (i.e., for a stronger ferromagnetic state). Due to the fact that our x-ray data (see Sec. III C) shows that, within the experimental error, the bulk modulus does not depend on the Co concentration  $x$ , a noticeable contribution of the lattice to the observed differences in the pressure dependence of  $T_M$  can be ruled out. A possible reason for the different pressure dependencies of  $T_M$  is crystallographic disorder, which is expected to increase with increasing Co concentration (see Sec. I).

In fact, atomic ordering has been shown to strongly affect the stability of the magnetic state in  $3d$  metallic ferromagnetic alloys; for example, the ferromagnetic state in the ordered phase of  $\text{Fe}_{72}\text{Pt}_{28}$  has been found to be more stable against external pressure than that in the disordered phase.<sup>45,46</sup> This case, however, is somehow different than that in  $\text{Fe}_{1-x}\text{Co}_x\text{Si}$ : in  $\text{Fe}_{72}\text{Pt}_{28}$  (fcc,  $\text{Cu}_3\text{Au}$ -type structure) order and disorder are directly connected with a change of the average number of the Fe nearest neighborhood and thereby directly affect the strength of the ferromagnetic state and its stability against pressure.<sup>45,46</sup> In the case of  $\text{Fe}_{1-x}\text{Co}_x\text{Si}$  with the B20-type structure, doping with Co induces disorder in the next nearest neighborhood of Fe and the atomic sizes of Fe and Co do not differ much. Indeed, this crystallographic disorder is much less than that of disordered  $\text{Fe}_{72}\text{Pt}_{28}$ . However, as we mentioned in Sec. I, doping with Co results in a local crystallographic disorder which has been detected by Raman spectroscopy.<sup>9</sup> Here, the linewidth of the Raman phonon has been found to be sensitive to disorder. At low temperatures ( $T = 5$  K) it shows a systematic change with increasing Co concentration  $x$ . The largest linewidth is observed for  $x = 0.5$ , which has the highest substitutional disorder. For  $x \geq 0.5$  it decreases gradually as disorder decreases. It has to be mentioned here that such local crystallographic disorder is on a much shorter length scale than that typical for x-ray diffraction and, therefore, it cannot be detected on a long length scale. The most important consequence of such local crystallographic disorder in  $\text{Fe}_{1-x}\text{Co}_x\text{Si}$  is that it strongly affects the magnetic structure<sup>10</sup> and is shown to weaken the

polarization of the ferromagnetic half-metallic state for  $x > 0.25$ .<sup>6</sup> In the following, we would like to relate the observed pressure dependence of  $T_M$  for the different concentrations to a corresponding change of the magnetic structure and character of the ferromagnetic half-metallic state.

Regarding the magnetic structure of  $\text{Fe}_{1-x}\text{Co}_x\text{Si}$ , it has been shown that, for small concentrations  $x \lesssim 0.15$ , the helix axis is nearly oriented along the  $\langle 100 \rangle$  direction due to the anisotropic exchange. However, the anisotropy of the system decreases with increasing Co concentration for  $x \geq 0.2$  and results in a distribution of the helix wave vector. This distribution has been shown to be random for high Co concentration ( $x = 0.5$ ).<sup>10</sup> On the other hand, *ab initio* calculations on  $\text{Fe}_{1-x}\text{Co}_x\text{Si}$  revealed that such local disorder at concentrations above  $x > 0.25$  is responsible for the decrease of the polarization of the ferromagnetic half-metallic state. This has been shown to be reflected in the deviation of the linear dependence of the magnetic moment on the concentration for  $x > 0.25$ .<sup>6</sup> Thus, at high concentrations, local disorder causes a decrease of the anisotropic exchange and weakens the character of the ferromagnetic half-metallic state. We thus would expect that the ferromagnetic state at low concentrations ( $x = 0.1$ ) is more robust against pressure than the state with higher concentrations ( $x = 0.2$  and  $0.3$ ). This scenario can explain the observed decrease of the stability of the ferromagnetic state under pressure as Co concentration increases. Indeed, the sample with the lowest local disorder ( $x = 0.1$ ) reveals the smallest pressure dependence of  $T_M$ ; that is, a higher stability of the ferromagnetic state when compared to that observed for the sample with higher concentrations ( $x = 0.3$ ). This finding is consistent with the above mentioned neutron diffraction studies<sup>10</sup> and *ab initio* calculations<sup>6</sup> on  $\text{Fe}_{1-x}\text{Co}_x\text{Si}$ , which show that the strength of the anisotropic exchange and the character of the half-metallic state remain unchanged for Co concentrations below  $x \leq 0.15$  and  $x \leq 0.25$ , respectively. In contrast, as the Co concentration exceeds these values, both the anisotropic exchange and the half-metallic character will be modified and result in an instability of the ferromagnetic state. This can explain our observation of a larger pressure-induced decrease of  $T_M$  for  $x = 0.3$  than that for  $x = 0.1$  and  $0.2$ . In the sample with  $x = 0.3$ , the instability of the ferromagnetic state originates from a decrease of both the anisotropic exchange and the half-metallic character. Both effects lead to the observed largest pressure dependence of  $T_M$ . The situation is different for the sample with  $x = 0.2$ . This is because, for concentrations  $x \leq 0.25$ , local disorder does not affect the half-metallic nature of the system.<sup>6</sup> In such a case ( $x = 0.2$ ) the stability of the ferromagnetic state can be only affected by a corresponding decrease of the anisotropic exchange and thus exhibits a smaller pressure dependence of  $T_M$  compared to that observed for the sample with  $x = 0.3$ . In this respect we would like to mention that the relative decrease of  $T_M$  with pressure ( $\frac{1}{T_M} \frac{\partial T_M}{\partial p}$ ) for the sample with  $x = 0.2$  ( $\frac{1}{T_M} \frac{\partial T_M}{\partial p} \sim 0.08 \text{ GPa}^{-1}$ ) is comparable with that of the sample with  $x = 0.1$  ( $\sim 0.09/\text{GPa}$ ) while the relative decrease of the sample with  $x = 0.3$  is noticeably larger ( $\sim 0.14/\text{GPa}$ ). This suggests that the character of the half-metallic state is the dominating factor for the observed differences of the pressure dependence of  $T_M$  in the doped samples.

## V. SUMMARY

The aim of the present high-pressure study was to investigate the pressure-induced quantum phase transitions (QPT) in ferromagnetic  $\text{Fe}_{0.9}\text{Co}_{0.1}\text{Si}$  ( $T_C \sim 11 \text{ K}$ ) and  $\text{Fe}_{0.8}\text{Co}_{0.2}\text{Si}$  ( $T_C \sim 32 \text{ K}$ ). This was motivated by the recently observed pressure-induced QPT in  $\text{Fe}_{0.7}\text{Co}_{0.3}\text{Si}$  ( $T_C \sim 43 \text{ K}$ ) and the associated unusual temperature dependence of the electrical resistivity [ $\rho(T) \propto T$ ] near the QPT,<sup>5</sup> suggested to be attributed to the atomic disorder of the sample. Since the samples with  $x = 0.1$  and  $x = 0.2$  are much less disordered, the present investigation should help establish whether disorder is responsible for the observed unusual  $\rho(T) \propto T$  behavior near the QPT.

To explore the magnetic ground state at ambient pressure of the investigated samples ( $x = 0.1, 0.2$ , and  $0.3$ ) at a microscopic level, we have applied  $^{57}\text{Fe}$  Mössbauer-effect spectroscopy. The results of the Mössbauer data revealed that the concentration dependence of the average magnetic hyperfine field at the  $^{57}\text{Fe}$  nucleus is proportional to the corresponding change of the macroscopic magnetic moment. Further analysis of the Mössbauer-effect data indicate that the onset of magnetic order in  $\text{Fe}_{1-x}\text{Co}_x\text{Si}$  is for  $x \gtrsim 0.05$ , which is consistent with previous reports from magnetization measurements.<sup>4,5</sup>

High-pressure resistivity measurements up to 30 GPa and 15 GPa for  $\text{Fe}_{0.9}\text{Co}_{0.1}\text{Si}$  and  $\text{Fe}_{0.8}\text{Co}_{0.2}\text{Si}$ , respectively, revealed in both samples a gradual suppression of the ferromagnetic state to a QPT at pressures of  $p \sim 11 \text{ GPa}$  and  $p \sim 12 \text{ GPa}$ , respectively. Energy dispersive x-ray diffraction measurements on  $\text{Fe}_{1-x}\text{Co}_x\text{Si}$  ( $x = 0.1, 0.2, 0.3$ ) indicated that the observed QPT are not connected with a structural phase transition. A comparison of the critical pressure for the QPT in the three samples indicates that the stability of the ferromagnetic state decreases with increasing Co concentration.

The analysis of all experimental results led to the following conclusions: The suppression of the ferromagnetic state is not related to a structural instability of the samples but rather strongly coupled to their different degree of local crystallographic disorder. However, in the pressure-induced nonmagnetic metallic state, local crystallographic disorder does not seem to affect the observed non-Fermi liquid behavior with  $\rho(T) \propto T$ . This clearly indicates that the unusual behavior (exponent  $n \sim 1$ ) is not due to the existence of local crystallographic disorder but is characteristic of the metallic high-pressure state of  $\text{Fe}_{1-x}\text{Co}_x\text{Si}$  with  $x = 0.1, 0.2, 0.3$  near and beyond the QPT. The observed positive magnetoresistance in the high-pressure state of  $\text{Fe}_{0.9}\text{Co}_{0.1}\text{Si}$  could be attributed to a slight field-induced modification of the spin majority and minority bands which leads to a very small magnetic moment.

## ACKNOWLEDGMENTS

This work was financially supported by the Deutsche Forschungsgemeinschaft (DFG) through SFB 608 and a joint project of DFG and the South African National Research Foundation (NRF). M.K.F. and M.M.A. thank A. Rosch and E. Bauer for fruitful discussions.

- <sup>1</sup>M. A. Chernikov, L. Degiorgi, E. Felder, S. Paschen, A. D. Bianchi, H. R. Ott, J. L. Sarrao, Z. Fisk, and D. Mandrus, *Phys. Rev. B* **56**, 1366 (1997).
- <sup>2</sup>J. Beille, J. Voiron, F. Towfiq, M. Roth, and Z. Y. Zhang, *J. Phys. F: Metal Phys.* **11**, 2153 (1981).
- <sup>3</sup>J. Beille, J. Voiron, and M. Roth, *Solid State Commun.* **47**, 399 (1983).
- <sup>4</sup>N. Manyala, Y. Sidis, J. F. DiTusa, G. Aeppli, D. P. Young, and Z. Fisk, *Nature (London)* **404**, 581 (2000).
- <sup>5</sup>Y. Onose, N. Takeshita, C. Terakura, H. Takagi, and Y. Tokura, *Phys. Rev. B* **72**, 224431 (2005).
- <sup>6</sup>J. Guevara, V. Vildosola, J. Milano, and A. M. Llois, *Phys. Rev. B* **69**, 184422 (2004).
- <sup>7</sup>F. P. Mena, J. F. DiTusa, D. van der Marel, G. Aeppli, D. P. Young, A. Damascelli, and J. A. Mydosh, *Phys. Rev. B* **73**, 085205 (2006).
- <sup>8</sup>D. Menzel, P. Popovich, N. N. Kovaleva, J. Schoenes, K. Doll, and A. V. Boris, *Phys. Rev. B* **79**, 165111 (2009).
- <sup>9</sup>A.-M. Racu, D. Menzel, J. Schoenes, and K. Doll, *Phys. Rev. B* **76**, 115103 (2007).
- <sup>10</sup>S. V. Grigoriev, V. A. Dyadkin, D. Menzel, J. Schoenes, Y. O. Chetverikov, A. I. Okorokov, H. Eckerlebe, and S. V. Maleyev, *Phys. Rev. B* **76**, 224424 (2007).
- <sup>11</sup>V. Jaccarino, G. K. Wertheim, J. H. Wernick, L. R. Walker, and S. Arajs, *Phys. Rev.* **160**, 476 (1967).
- <sup>12</sup>B. Buschinger, C. Geibel, F. Steglich, D. Mandrus, D. Young, J. L. Sarrao, and Z. Fisk, *Physica B* **230-232**, 784 (1997).
- <sup>13</sup>Z. Schlesinger, Z. Fisk, H.-T. Zhang, M. B. Maple, J. F. DiTusa, and G. Aeppli, *Phys. Rev. Lett.* **71**, 1748 (1993).
- <sup>14</sup>A. Damascelli, K. Schulte, D. van der Marel, and A. A. Menovsky, *Phys. Rev. B* **55**, R4863 (1997).
- <sup>15</sup>H. Watanabe, H. Yamamoto, and K. Ito, *J. Phys. Soc. Jpn.* **18**, 995 (1963).
- <sup>16</sup>G. K. Wertheim, V. Jaccarino, J. H. Wernick, J. A. Seitchik, H. J. Williams, and R. C. Sherwood, *Phys. Lett.* **18**, 89 (1965).
- <sup>17</sup>G. Aeppli and Z. Fisk, *Comments Condens. Matter Phys.* **16**, 155 (1992).
- <sup>18</sup>D. Zur, D. Menzel, I. Jursic, J. Schoenes, L. Patthey, M. Neef, K. Doll, and G. Zwicknagl, *Phys. Rev. B* **75**, 165103 (2007).
- <sup>19</sup>M. Klein, D. Zur, D. Menzel, J. Schoenes, K. Doll, J. Röder, and F. Reinert, *Phys. Rev. Lett.* **101**, 046406 (2008).
- <sup>20</sup>M. Klein, D. Menzel, K. Doll, M. Neef, D. Zur, I. Jursic, J. Schoenes, and F. Reinert, *New J. Phys.* **11**, 23026 (2009).
- <sup>21</sup>Y. Ishikawa, K. Tajima, D. Bloch, and M. Roth, *Solid State Commun.* **19**, 525 (1976).
- <sup>22</sup>M. Ishida, Y. Endoh, S. Mitsuda, Y. Ishikawa, and M. Tanaka, *J. Phys. Soc. Jpn.* **54**, 2975 (1985).
- <sup>23</sup>L. Lundgren, O. Beckman, V. Attia, S. P. Bhattacharjee, and M. Richardson, *Phys. Scr.* **1**, 69 (1970).
- <sup>24</sup>B. Lebech, J. Bernhard, and T. Freltoft, *J. Phys. Condens. Matter* **1**, 6510 (1989).
- <sup>25</sup>C. Pfleiderer, G. J. McMullan, S. R. Julian, and G. G. Lonzarich, *Phys. Rev. B* **55**, 8330 (1997).
- <sup>26</sup>N. Doiron-Leyraud, I. R. Walker, L. Taillefer, M. J. Steiner, S. R. Julian, and G. G. Lonzarich, *Nature (London)* **425**, 595 (2003).
- <sup>27</sup>P. Pedrazzini, D. Jaccard, G. Lapertot, J. Flouquet, Y. Inada, H. Kohara, and Y. Onuki, *Physica B* **378-380**, 165 (2006).
- <sup>28</sup>P. Pedrazzini, H. Wilhelm, D. Jaccard, T. Jarlborg, M. Schmidt, M. Hanfland, L. Akselrud, H. Q. Yuan, U. Schwarz, Y. Grin, and F. Steglich, *Phys. Rev. Lett.* **98**, 047204 (2007).
- <sup>29</sup>K. Syassen, *High Press. Res.* **28**, 75 (2008).
- <sup>30</sup>R. Boehler and K. De Hantsetters, *High Pressure Res.* **24**, 391 (2004).
- <sup>31</sup>D. L. Heinz and R. Jeanloz, *J. Appl. Phys.* **55**, 885 (1984).
- <sup>32</sup>F. Porsch, EDXPowd 3.155, Windows Version, RTI GmbH Paderborn, Germany (1996).
- <sup>33</sup>G. K. Wertheim, J. H. Wernick, and D. N. E. Buchanan, *J. Appl. Phys.* **37**, 3333 (1966).
- <sup>34</sup>N. Blaes, H. Fisher, and U. Gonser, *Nucl. Instrum. Methods B* **9**, 201 (1985).
- <sup>35</sup>M. Fanciulli, A. Zenkevich, I. Wenneker, A. Svane, N. E. Christensen, and G. Weyer, *Phys. Rev. B* **54**, 15985 (1996).
- <sup>36</sup>R. A. Brand, *WinNormos-for-Igor Users Manual*, WissEl GmbH, Starnberg (Universität Duisburg, Duisburg, 2006).
- <sup>37</sup>A. Mani, A. Bharathi, and Y. Hariharan, *Phys. Rev. B* **63**, 115103 (2001).
- <sup>38</sup>R. L. Mills, B. Olinger, and D. T. Cromer, *J. Chem. Phys.* **84**, 2837 (1986).
- <sup>39</sup>F. D. Murnaghan, *Am. J. Math.* **59**, 235 (1937).
- <sup>40</sup>C. Pfleiderer, D. Reznik, L. Pintschovius, H. v. Löhneysen, M. Garst, and A. Rosch, *Nature (London)* **427**, 227 (2004).
- <sup>41</sup>J. A. Hertz, *Phys. Rev. B* **14**, 1165 (1976).
- <sup>42</sup>T. Moriya, *Spin Fluctuations in Itinerant Electron Magnetism* (Springer, Berlin, 1985).
- <sup>43</sup>A. J. Millis, *Phys. Rev. B* **48**, 7183 (1993).
- <sup>44</sup>K. Ishimoto, M. Ohashi, H. Yamauchi, and Y. Yamaguchi, *J. Phys. Soc. Jpn.* **61**, 2503 (1992).
- <sup>45</sup>M. M. Abd-Elmeguid and H. Micklitz, *Physica B: Condensed Matter* **163**, 412 (1990).
- <sup>46</sup>M. M. Abd-Elmeguid, *Nucl. Instrum. Methods B* **76**, 159 (1993).